PCCP

Accepted Manuscript

This is an *Accepted Manuscript*, which has been through the Royal Society of Chemistry peer review process and has been accepted for publication.

Accepted Manuscripts are published online shortly after acceptance, before technical editing, formatting and proof reading. Using this free service, authors can make their results available to the community, in citable form, before we publish the edited article. We will replace this *Accepted Manuscript* with the edited and formatted *Advance Article* as soon as it is available.

You can find more information about *Accepted Manuscripts* in the **Information for Authors**.

Please note that technical editing may introduce minor changes to the text and/or graphics, which may alter content. The journal's standard **Terms & Conditions** and the **Ethical guidelines** still apply. In no event shall the Royal Society of Chemistry be held responsible for any errors or omissions in this *Accepted Manuscript* or any consequences arising from the use of any information it contains.

An Infrared Spectroscopic and Theoretical Study on $(CH_3)_3N\text{-}H^+\text{-}(H_2O)_n$, $n = 1 – 22$: Highly Polarized Hydrogen Bond Networks of Hydrated Clusters

Ryunosuke Shishido,[1] Ying-Cheng Li,,[2,3] Chen-Wei Tsai,[2,3] Dan Bing[4], Asuka Fujii,*[1]

and Jer-Lai Kuo*[3]

Department of Chemistry, Graduate School of Science,

Tohoku University, Sendai 980-8578, Japan

Department of Physics, National Taiwan University, Taipei 10617, Taiwan

Institute of Atomic and Molecular Sciences, Academia Sinica, Taipei, 10617, Taiwan

Pujiang Institute, Nanjing Tech University, Nanjing, 211134, China

* To whom corresponding should be addressed.

E-mail: asukafujii@m.tohoku.ac.jp (A.F.), jlkuo@pub.iams.sinica.edu.tw (J.-L.K.).

[1] Tohoku University, [2] National Taiwan University, [3]Academia Sinica, [4]Nanjing Tech University

Abstract

Infrared spectra of protonated trimethylamine (TMA) - water clusters,

$(CH_3)_3N\text{-}H^+\text{-}(H_2O)_n$ ($n = 1 - 22$) were measured in the OH stretching vibrational

region by size-selective photodissociation spectroscopy. Density functional theory

calculations of stable structures were performed, and temperature dependence of the

isomer populations and infrared spectra was also simulated by the harmonic

superposition approximation approach to analyze hydrogen bond network structures in

the clusters. It was shown that the excess proton (H^+) in this system localizes on the

TMA moiety regardless of cluster size. In the small-sized clusters, many isomers

coexist and their hydrogen bond networks are highly polarized to induce the large

charge-dipole interaction to stabilize the excess proton. Magic number behavior is not

observed at around the magic number size ($n = 21$) of protonated water clusters and its

implication on the hydrogen bond network structures is discussed.

I. Introduction

The large magnitude of the permittivity of water is explained not only by the dipole moment of the monomer (1.85 D) [1] but also the high flexibility of its hydrogen bond (H-bond) network structures. In the hydration of a charged species, the orientation of water molecules around the charged species is arranged to form a highly polarized H-bond network which stabilizes the system. [2, 3] Such a network structure would be governed by the balance between the stability of the network itself and the magnitude of the net dipole moment of the water network. Gas phase cluster studies can provide us a microscopic picture on the formation of such a highly polarized H-bond network under the influence of a charged species. A number of spectroscopic and theoretical studies on hydrated cation/anion clusters have been reported, and a variety of water H-bond network structures have been found. [4 - 15] When a water network is in contact with a charged species through only a single water site, the feature of the polarized water network would be most prominent. An example is the small water anions $(H_2O)_{5,6}^-$, of which H-bond networks are obviously arranged to produce the large net dipole moment for the binding of the excess electron. [16] Such an example, however, has been rarely found in hydration of cations or protonated species because multiple coordination is formed (this is typical in hydration of metal cations) or intra-cluster proton transfer to

the water moiety occurs with increasing cluster size. [4-20]

To study the microscopic nature of highly polarized water networks, protonated trimethylamine-water clusters TMA-H$^+$-(H$_2$O)$_n$ are of great interest.   In H-bond networks, TMA can play only the role of a single proton acceptor.   If the excess proton (H$^+$) is localized at TMA because of its much larger proton affinity (PA, 227 kcal/mol) than that of water (165 kcal/mol), [21] the protonated TMA site acts as a single proton donor and can directly contact only with a single water site in the water network.   Thus the protonated TMA site is located at a terminal site of the water network, and the water network is expected to be highly polarized to stabilize the charge in the excess proton. This cluster system will be useful to explore how large net dipole moment can be formed by water networks. With increasing order of the solvation shells, the water network in solvation shells away from the excess proton will eventually become non-polarized. The TMA-H$^+$-(H$_2$O)$_n$ clusters will provide insight on this microscopic dielectric shielding.

In the case of protonated binary-component clusters X-H$^+$-(Y)$_n$, the preferential location of the excess proton is not actually evident because not only the difference between the PAs of the two components (X and (Y)$_n$) but also the mutual solvation energy govern the preferential location of the excess proton. [17 - 20, 22 - 27] Very recently,

we have studied the preferential location of the excess proton in TMA-H^+-$(CH_3OH)_n$ by using the theoretical and experimental approaches and we have shown that though PA of $(CH_3OH)_n$ at $n \geq 6$ becomes larger than that of TMA, the preferential location of the excess proton is the TMA moiety regardless of the cluster size. [27] The PA of water (165 kcal/mol) is lower than that of methanol (180 kcal/mol). [21] Therefore, it is expected that in TMA-H^+-$(H_2O)_n$ the excess proton is localized on the TMA moiety. We have studied the structure of TMA-H^+-$(H_2O)_1$ by infrared (IR) spectroscopy and density functional theory (DFT) calculations and have confirmed the unique protonation to the TMA moiety. [28] For the much larger sized region, Chang *et al.* have recently reported IR spectra of TMA-H^+-$(H_2O)_n$ around the magic number size of protonated water clusters $H^+(H_2O)_n$. [29] On the basis of the observation of the magic number behavior at $n = 20$ and the comparison with IR spectra of related hydrated clusters, the presence of two or more structural families and the surface location of the charged site have been concluded. However, the preferential site of the excess proton (H^+TMA core or hydronium ion) has not clearly been determined.

In the present study, we observe IR spectra of TMA-H^+-$(H_2O)_n$ ($n = 1 - 22$) in the OH stretching vibrational region to examine their H-bond network structures. To support the structure determination of the clusters, stable structures, relative energies,

5

and temperature dependence of the isomer populations and vibrational spectra are calculated by the DFT method. In addition, to determine the location of the excess proton, we compare the observed spectra with those of $H^+(H_2O)_n$ at the same size. The features of the polarized H-bond networks of water are discussed.

II. Methodology

Experimental

IR spectra of TMA-H^+-$(H_2O)_n$ (n = 1 – 22) were recorded using IR predissociation spectroscopy with a mass spectrometer equipped with linearly aligned tandem quadrupole mass filters connected by an octopole ion guide. Details of the experimental apparatus have been described elsewhere [27, 28] and only brief description is given here. TMA-H^+-$(H_2O)_n$ was produced by pulsed discharge of a TMA / H_2O mixed vapor seeded in Ar buffer gas (total stagnation pressure of 5 atm). The gaseous mixture was expanded from a pulsed supersonic jet valve (General Valve series #9). A pin electrode was installed beside the nozzle and a pulsed voltage of ~400 V relative to the nozzle was applied to the electrode. The voltage pulse width was 40 μs. Application of the high voltage pulse was synchronized with the pulsed valve operation. Ionization by the discharge and successive proton transfer generated protonated species. Intensities of

unprotonated ionic species were negligible under the present source condition. TMA-H$^+$-(H$_2$O)$_n$ clusters were produced and cooled by the jet expansion. The cluster of interest was size-selected by the first quadrupole mass filter and then was introduced into the octopole ion guide. The mass resolution of the first mass filter was set to be sufficiently high ($\Delta m/Z \leq \sim 1$) to prevent contamination by other cluster species. Within the octopole ion guide, the size-selected cluster was irradiated with counter propagating IR laser light, and was sent to the second quadrupole mass filter, which was tuned to pass only the mass of the TMA-H$^+$-(H$_2$O)$_{n\text{-1 or }n\text{-2}}$ fragment ion produced by vibrational excitation. Thus, an IR spectrum of the size-selected cluster was recorded by monitoring the fragment ion intensity while scanning the IR laser frequency. The TMA-loss channel was negligible compared with the water-loss channels. Coherent IR light was generated by an IR optical parametric oscillator (Laser Vision) pumped with the fundamental output of a YAG laser (Continuum Inc., Powerlite 8000). Because of the limitation of the output power in the low-frequency region, reliable measurements were restricted above 2400 cm^{-1} in this experiment. All the observed spectra were normalized according to the IR power. The nearly linear laser power dependence of the fragmentation signal was confirmed. The spectra were calibrated to the vacuum wavenumber by simultaneous observation of atmospheric water absorption lines. In

addition, for a comparison, we measured IR spectra of $H^+(H_2O)_n$ by using the same method and ion source.

Theoretical Calculations

Based on the previous discussions, the water H-bond network of $TMA\text{-}H^+\text{-}(H_2O)_n$ is expected to differ from both their neutral and protonated counterparts. The difference of H-bond network of these two species has been thoroughly examined in the previous studies on $(H_2O)_n$ and $H^+(H_2O)_n$. [30, 31] Thus, initial structures of $TMA\text{-}H^+\text{-}(H_2O)_n$ for $n \leq 6$ can be generated either by adding TMA to the free OH site of protonated water clusters $(H^+(H_2O)_n)$ or by adding a protonated TMA $(TMA\text{-}H^+)$ to a lone pair orbital of neutral water clusters $((H_2O)_n)$. All structures are optimized first by B3LYP/6-31+G* as this exchange-correlation functional has been used extensively to study protonated water clusters and the small basis-set used also allows a quick convergence in geometry optimization. [32] For $n = 1$ and 2, only one isomer is found and for $n = 3$, there are only two stable isomers. For $n = 4$ to 6, we found 14, 87, and 638 isomers, respectively, by B3LYP/6-31+G*. For $n = 5$ and 6, we found isomers with proton transfer to the water moiety, but their relative energies are at least 12 kcal/mol higher than the most stable forms. Due to the exponential growth of stable minima with respect to size, our search

scheme is limited to size $n \leq 6$. Details of these results can be found in Electronic

supplementary information (ESI).

Three bulky methyl groups in TMA deserve a close check on the role of

dispersion, thus we engage ωB97xD/6-311+G(2d,p) to further relax the geometry of

these clusters and to get the final energetics and vibrational spectra. [33] Similar to the

previous study on TMA-H$^+$-(MeOH)$_n$, [27] we did not find significant difference between

B3LYP/6-31+G* and ωB97xD/6-311+G(2d,p). Comparison between these two

exchange-correlation functionals can be found in ESI. In the main text, we only use

results derived from ωB97xD/6-311+G(2d,p). All the calculations were performed by

the Gaussian 09 program suite. [34] Calculated stable structures were visualized by the

MOLKEL program. [35]

For n = 1 - 3, we compare DFT calculated spectra directly with experimental

data. For $n \geq 4$, however, there exist so many isomers that we need to count on

analyzing the averaged population of all isomers at different temperatures. Assuming

the thermal equilibrium, we can calculate the canonical probability $P_a(T)$ of the isomer a

by employing the harmonic approximation. [27, 36] Under the quantum harmonic

superposition approximation (Q-HSA), $P_a(T)$ is written as $P_a(T) = \dfrac{Z_a(\beta)}{Z(\beta)}$, where,

$$Z_a(\beta) = \exp(-\beta E_a) \prod_f \frac{\exp(-\beta \hbar \omega_f^a / 2)}{1 - \exp(-\beta \hbar \omega_f^a)}, \quad Z(\beta) = \sum_a n_a Z_a(\beta), \quad \text{and} \quad \beta \equiv \frac{1}{k_B T} \quad \text{is the}$$

"inverse temperature". E_a is the electronic energy, and ω_f^a is the f-th vibrational

frequency of isomer a. Furthermore, the IR spectra are synthesized by the

statistically-weighted contributions of all the isomers. The total temperature dependent

IR spectrum intensity can be expressed as $I_{total}(\omega, T) = \sum_a I_a(\omega) P_a(T)$, where the

$I_a(\omega)$ is the spectrum intensity in harmonic frequencies calculations. For the

homogeneous width, we broden free OH and CH streching modes with 20 and 5 cm^{-1},

respectively. For the H-bonded OH stretching, we adopt the power law formula

proposed by Takahashi and co-worker derived from studying the vibrational decay

lifetime of the OH bond stretch. [37, 38] They found the homogeneous width for the

intramolecular hydrogen-bonded OH stretch can be written as $\Gamma = \alpha(\omega_{freeOH} - \omega)^\beta$,

where $\Delta\omega$ is the red shift of the H-bonded OH band peak with respect to the free OH

peaks in the experimental spectra. All the units of Γ and $\Delta\omega$ are chosen in

wavenumber (cm^{-1}). Following our previous studies on protonated methanol clusters, [36]

the α and β value we used here are $\alpha = 0.0009$ and $\beta = 1.9$. The ω_{freeOH} value is

3750 cm^{-1} and all harmonic frequencies are rescaled by 0.9394 to be compared with

experimental data.

III. Results and discussion

1. IR spectra of TMA-H$^+$-(H$_2$O)$_n$ (n = 1-10) in the free OH stretch region

Figure 1 shows the comparison of the observed IR spectra of size-selected (a) TMA-H$^+$-(H$_2$O)$_n$ (n = 1-10) and (b) H$^+$(H$_2$O)$_n$ (n = 4 - 10) in the free OH stretch region. Each spectrum was measured by monitoring the TMA-H$^+$-(H$_2$O)$_{n-1}$ or H$^+$(H$_2$O)$_{n-1}$ fragment while scanning the IR wavelength.

The IR spectra of H$^+$(H$_2$O)$_n$ shown in Figure 1 are essentially same as those reported previously. [32, 39 - 43] It has been demonstrated that the free OH stretch region of protonated water–containing clusters is a sensitive probe of the H-bonding environment and network morphology. [6, 7, 9 – 15, 32, 39 – 45] If the excess proton is localized at the water moiety, IR spectra of TMA-H$^+$-(H$_2$O)$_n$ should be similar to those of H$^+$(H$_2$O)$_n$. [43] However, the observed spectra of TMA-H$^+$-(H$_2$O)$_n$ are clearly different from those of H$^+$(H$_2$O)$_n$. This observation means that the excess proton in TMA-H$^+$-(H$_2$O)$_n$ is localized at the TMA moiety within this size range and their H-bond networks in the water moiety are different from those of H$^+$(H$_2$O)$_n$.

Prior to the discussion on the structures of TMA-H$^+$-(H$_2$O)$_n$, here we briefly summarize the correlation between the free OH stretch frequency and the H-bond coordination number of water, that has been established in H$^+$(H$_2$O)$_n$ and many hydrated

clusters with an excess proton. [32, 39 – 45] A water molecule which is located at a terminal of a H-bond chain is a single proton acceptor (A) site, and its symmetric (ν_1) and antisymmetric (ν_3) stretching vibrational bands of the free OH bonds appear at ~3640 and ~3740 cm^{-1}, respectively. An H-bond linear chain is composed of two-coordinated water molecules, which are single acceptor–single donor (AD) sites. Their free OH stretch bands appear at ~3715 cm^{-1}. A three-coordinated water molecule in a double acceptor-single donor (AAD) site also has a free OH bond and its stretching vibration band is seen at ~3695 cm^{-1}. Such an AAD site appears at a branching point of an H-bond network.

In the observed IR spectra of TMA-H$^+$-(H$_2$O)$_n$, the ν_1 and ν_3 bands of A sites appear in $n = 1 – 5$ (labeled by the green dotted lines in Figure 1). But both the bands completely disappear in $n \geq 6$. This means that the H-bond network structures have transformed from open chain types to closed ring types at $n = 6$. On the other hand, in H$^+$(H$_2$O)$_n$, the disappearance of the ν_1 and ν_3 bands occurs at $n \sim 10$. [39 - 42] This result indicates that TMA-H$^+$-(H$_2$O)$_n$ forms a closed ring network at much smaller sizes than H$^+$(H$_2$O)$_n$. The free OH stretching band of AD sites appears at ~3715 cm^{-1} (labeled by the blue dotted lines) and this band is located in between the two bands of the A sites. In the spectra of TMA-H$^+$-(H$_2$O)$_n$, the AD band seems to show a small shift to *lower*

frequency at $n = 6$. Though free OH bands of $H^+(H_2O)_n$ also show a frequency shift trend with increasing cluster size, their shifts are toward *higher* frequency due to the dilution of the excess charge effect. Therefore, the band shift at $n = 6$ is attributed to the appearance of a new band at the low frequency side of the AD band. This new band should be attributed to three-coordinated AAD sites (labeled by the red dotted line). The presence of a weak shoulder in the band, which corresponds to the AD site, also supports this assignment. Then it is concluded that the separation of the AD and AAD bands in TMA-H^+-$(H_2O)_n$ is much smaller than that in $H^+(H_2O)_n$.

All of these spectral features in the free OH stretch region demonstrate that the excess proton in TMA-H^+-$(H_2O)_n$ is localized at the TMA moiety in the size range of $n = 1 – 10$ and the water moiety should be neutral. However, the band features of TMA-H^+-$(H_2O)_n$ are also different from those of neutral water clusters $(H_2O)_n$. [46, 47] In particular, we should note that the splitting between the two and three-coordinated water bands is not observed in $(H_2O)_n$ and neutral hydrated clusters. [46 - 51] Therefore, we conclude that the H-bond network of TMA-H^+-$(H_2O)_n$ is neutral but is under the strong influence of the excess proton. We also note that the localization of the excess proton in the TMA moiety has been also concluded for TMA-H^+-$(MeOH)_n$ ($n = 3 – 7$), in which the proton affinity of the methanol moiety in $n \geq 4$ is expected to be larger than

TMA. [27]

2. IR spectra of TMA-H$^+$-(H$_2$O)$_n$ (n = 1-10) in the H-bonded OH stretch region

To obtain more detailed information on the H-bond network structures of

TMA-H$^+$-(H$_2$O)$_n$, we observed IR spectra in the H-bonded OH stretch region. The

observed spectra of n = 1 – 10 are reproduced in Figure 2. In addition to the relatively

sharp bands of the free OH stretches above 3600 cm^{-1}, broadened bands are seen in the

3000 – 3600 cm^{-1} region in the spectra of n > 1, and they are attributed to the H-bonded

OH stretches in the water moiety. The stretching vibration band of the excess proton

appears at the 2800 -3200 cm^{-1} region in the spectrum of n = 1 (as discussed below). [28]

With increasing cluster size, this band largely shifts to lower frequency and only its tail

of the high frequency side can be seen in $n \geq 4$. In the following, we will discuss the

cluster structure of n = 1 - 6 on the basis of the comparison between the observed IR

spectra and their simulations.

The observed IR spectrum of TMA-H$^+$-(H$_2$O)$_1$ is reproduced in Figure 3(a).

Since this spectrum has been already reported in our other paper, [28] we only briefly

review the results. The two bands at 3637 and 3730 cm^{-1} are assigned to the ν_1 and ν_3

free OH stretching modes, respectively. Broadened bands at 2800 and 3100 cm^{-1}are

attributed to the Fermi resonance between the N-H$^+$ stretching mode and the overtones

of the N-H$^+$ bending modes. The $n = 1$ cluster has a unique stable structure **1I** shown in Figure 3(b). In this structure, the excess proton is located at the TMA moiety. Even if the optimization starts with the excess proton on the water moiety, the excess proton is transferred to the TMA moiety during the optimization.

In the observed spectrum of $n = 2$ (Figure 3(c)), the free OH stretching bands appear at 3640 ~ 3750 cm^{-1} and an H-bonded OH stretching band is seen at 3400 cm^{-1}. Another intense band at 2775 cm^{-1} is assigned to the N-H$^+$ stretching band. In addition, some extra bands appear in the spectrum and they are attributed to Fermi mixing. Detailed analysis of this Fermi mixing is beyond the focus of the present paper.   The optimized structure **2I** shown in Figure 3(d) is a unique stable structure for $n = 2$.   In **2I**, the two water molecules form an H-bonded linear chain, which is bound to the excess proton.   The simulated IR spectrum well agrees with the observed IR spectrum except the appearance of the overtone/combination bands due to the Fermi mixing.

In the spectrum of TMA-H$^+$-(H$_2$O)$_3$ reproduced in Figure 3(e), the free OH stretch region shows three bands assigned to the pair of the ν_1 and ν_3 bands (A bands) and AD band.   An intense H-bonded OH stretch band appears at 3460 cm^{-1} and broaden features, which are attributed to H-bonded OH stretch and overtone/combinations, are also seen in 3000 − 3400 cm^{-1}.   The intense band at 2680

cm^{-1} is assigned to the N-H$^+$ stretching band. Two stable structures, **3I** and **3II** in Figure

3(f) and (g), respectively, were found for $n = 3$.   In both the structures, the excess

proton is localized at the TMA moiety. The water network is a linear chain in **3II** while

it is a tree (branched chain) type in **3I**. The observed spectrum shows a clear AD band in

the free OH stretch region, and this band can be reproduced only by **3II**.   On the other

hand, **3I** is more stable than **3II** though their energy difference is quite small (0.31

kcal/mol). Except the AD band, both the isomers show similar features, and

contributions of these isomers cannot be distinguished. Therefore, coexistence of both

the isomers is suggested.

As shown in Figure 2, the stretching vibration of the excess proton (the N-H$^+$

stretching mode) shows the shift trend to lower-frequency with increasing n, at least up

to $n = 3$.   In the $n \geq 4$ clusters, a broadened feature, which would be attributed to the

tail of the further shifted proton vibration band, is seen in the region below 2800 cm^{-1}.

Thus we focus on the free and H-bonded OH stretch bands above 3000 cm^{-1} to

determine the cluster structures and the excess proton location.   Number of stable

structures drastically increases in the $n \geq 4$ clusters, and unique structure determination

becomes difficult.   This is also because coexistence of multiple isomers is highly

plausible due to the thermal energy of the protonated clusters produced by the discharge

source. Thus, in $n \geq 4$, we employ the HSA approach to evaluate the averaged populations and simulate their IR spectra at different temperatures. [27, 36]

In addition to linear chain and tree type structures, single ring (SR) type structures become possible from $n = 4$. The temperature dependence of the isomer population of $n = 4$ calculated by the HSA approach is shown in Figure 4. The most stable structure is the linear chain type, and the rise of the contribution of the tree and single ring types is seen at $T = 50 - 100$ K, though their contribution is rather minor even for temperatures higher than 200 K. Moreover, in all the isomers, the excess proton is located at the TMA moiety. The IR simulations are compared with the observed spectrum in Figure 5. Since the temperature range of protonated clusters produced by the same ion source (e.g., TMA-H$^+$(CH$_3$OH)$_n$ and H$^+$(CH$_3$OH)$_n$) has been shown to be $150 - 200$ K, [27, 36] we focus on the comparison with the IR simulations below 200 K. Because of the dominant contribution of the linear chain isomers in $T \leq 200$ K, the temperature dependence of the simulated spectra is moderate and the free OH stretch bands above the 3600 cm^{-1} region shows a reasonable agreement with the observed spectrum in the entire temperature range we simulated. However, the gradual rise of the H-bonded OH stretch band at ~3500 cm^{-1} occurs with elevation of temperature, and better agreement with the observed spectrum is found at $T = 150 - 200$ K. Therefore,

the observed spectrum is interpreted by the linear chain type isomers with the minor

contribution of the tree and single ring isomers.   The structure of the global minimum

isomer with those of the most populated isomer in each morphology type at 200 K is

displayed in Figure 6. We should note that the water networks in all these isomers are

arranged to form a large net dipole moment to stabilize the charge at the excess proton.

In addition to the linear chain, tree, and single ring types, a more complicated

H-bond network type can be constructed in $n = 5$.   This is the double ring (DR) type,

which is formed by bridging two sites in a single ring network with H-bonds.   A

further comiplicated type, multiple ring (MR) type, in which more than two rings are

involved in the H-bond network, is also possible.   At $n = 5$, stable isomers with the

protonated water ion core are found.   They are, however, much less stable (at by least

12 kcal/mol) than the protonated TMA ion core isomers (details can be found in ESI).

The tempeature dependence of the isomer type population is shown in Figure 7.

Different from $n = 4$, the most stable isomer is a single ring type, and the population of

this type of isomers is dominant up to ~120 K. With elevation of temperature, however,

the linear chain type becomes competitive, and the change of the major component

occurs at ~220 K.   This is because the linear chain type is more flexible and has lower

frequency intermolecular vibration modes. Therefore, the entropy factor of the free

18

energy drives the population of the linear chain type in higher temperature. [36]

Contributions of the tree isomer type are almost negligible in $T \leq 200$ K.   In $n = 5$, the

relative energies of the double and multiple ring types are rather high because of the

large distortion of the H-bonds, and their rigid structures (higher intermolecular

vibrational frequencies) reduce their vibrational state density.   Therefore, the

populations of these types are negligible in the whole calculated temperature range.

The simulated IR spectra are shown in Figure 8.   The H-bond ring moiety in the single

ring type isomers has no A site (or these isomers can contain only one A site as a

dangling site to the ring moiety). Therefore the intensities of the v_1 and v_3 bands of the

A site are suppressed in the low temperature. With elevation of temperature, these two A

site bands become prominent because of the rise of the contribution of the linear chain

type isomers. In the H-bonded OH stretch band region, the band around 3500 cm^{-1}

occurs from the contribution of the linear chain isomers.   The observed spectra is best

reproduced by the simulation at 150 - 200 K, in which the population of the single ring

isomers is still dominant but the linear chain type isomers also occupy about 1/3 -1/2 of

the population.   The structure of the global minimum isomer with those of the most

populated isomer in each morphology type at 200 K is displayed in Figure 6.   Not only

the linear isomer but also the single ring isomer has the H-bond network arrangement to

induce large dipole moment to stabilize the charge on the excess proton in the TMA site.

The temperature dependence of the isomer population in $n = 6$ is shown in Figure 9. Also in $n = 6$, stable isomers with the protonated water ion core are much less stable (at by least 12 kcal/mol) than the protonated TMA ion core isomers and their populations are negligible (details can be found in ESI). The double ring type is the most stable structure in $n = 6$, and the population of this type is dominant in $T \leq 200$ K. This contrasts with the case of $n = 5$. At $n = 6$, the double ring can be formed without large distortion of H-bonds, and the enthalpy factor drives the population of the double ring type in the low temperature. The rigid structures of the double ring type are, however, disadvantageous in the entropy factor, and at $T = \sim 180$ K, the rise of the population of the single ring type occurs. The contribution of the linear chain type also rises in higher temperature, but it is negligible in $T < 200$ K. In the observed spectrum of $n = 6$, the A site bands almost disappear and the free OH band of the AAD band is seen. In the double ring type isomers, the bridging sites of the two H-bond ring moieties become three-coordinated (AAD or ADD) sites. Therefore, the two spectral features in the observed spectrum are consistent with the double ring type isomers. As seen in Figure 10, the temperature dependence of the IR simulations of $n = 6$ is very minor in $T \leq 200$ K. This is because the dominance of the double ring isomer type in $T < \sim 180$ K.

All the IR simulations of $T \leq 200$ K well reproduce the observed spectrum. Though the observed cluster temperature cannot be determined by the comparison with the simulations, the temperature of 150 – 200 K is reasonably suggested by the results of the $n = 4$ and 5 clusters which are produced simultaneously. Moreover, we conclude that the observed spectrum is well interpreted by the dominance of the double ring type isomers with the minor contribution of the single ring type. The structure of the global minimum isomer with those of the most populated isomer in each morphology type at 200 K is displayed in Figure 6. At $n = 6$, we observed the dominance of the closed ring types. Closed ring networks are characteristic in small-sized neutral water clusters $(H_2O)_n$ $(n \geq 3)$, [46, 48 -50, 52, 53] however, such types are rarely seen small-sized hydrated clusters with an excess proton. [15, 32, 54 – 59.] Here we should note that in the present experimental condition, the vibrational temperture of the protonated clusters is much higher (150 - 200 K) than that of typical neutral clusters in a jet ($< \sim$100K). This suggests that even small water networks prefer closed cyclic strucutres up to $\sim$200 K if the water networks has no proton (hydronium ion).

As seen above, all the observed spectra were well simulated by the clusters with the protonated TMA ion core, and we conclude that the excess proton is localized at the TMA site at least up to $n = 6$. To stabilize the proton at the TMA site, i.e., the

edge of the water H-bond network, the network should be highly polarized. This is

actually seen in the minimum energy and/or most populated structures displayed in

Figures 3 and 6. For further analysis, we estimated the dipole moment of the water

moiety of the stable isomers by assigning δ and -2δ on the H-atom and O-atom of a

water molecule. (Here we should note that δ is an arbitrary value and this calculation is

to show how the dipole moments in the water molecules are summed or cancelled each

other. As a very rough evaluation, however, dipole moment of $1\times\delta$ (unit of length is Å)

can be considered to be on the same level with that of the water monomer, 1.85 D.) The

correlation between dipole moment of an isomer and its relative energy for $n = 1 - 6$ is

shown in Figure 11(a).

For $n = 1$ and 2, the dipole moments are 1.2δ and 2.3δ. The two isomers of $n = 3$

have dipole moments around 3δ. From the structures in Fig.3, we can see water

molecules in these small-sized isomers are all line-up in a directional manner. In the

structures of the most populated isomers $n = 4 - 6$, the alignment of the OH group to

stabilize the excess charge is seen at least up to the $3^{rd} \sim 4^{th}$ shell water and their dipole

moment are about 4δ.

Most of the isomers for $n = 4$ to 6 have fairly large dipole moment ($\sim 4\delta$) and there is

no clear correlation between the magnitude of dipole moment of the water moiety and

relative stability. Furthermore, we examine the dependence between the magnitudes of dipole with their morphology. In Fig. 11 (b), we show the results for $n = 6$ and the complete results for $n = 4$ and 5 can be found in ESI. The lack of dependence on the dipole moment with morphology in this size range means that the polarity of the water network is a key factor to form stable isomers in this system regardless of their morphology. Thus, we expect the H-bond networks at larger size clusters would also form similar types of networks with large net dipole moments. Then we discuss the feature at large size clusters at around $n = 21$ and the effects of the excess proton to the H-bond networks.

3.   IR spectra of large sized TMA-H$^+$-(H$_2$O)$_n$

Figure 12 shows the mass spectrum of TMA-H$^+$-(H$_2$O)$_n$ and H$^+$(H$_2$O)$_n$. This mass spectrum was obtained by the co-expansion of TMA and water in the Ar carrier and both the protonated cluster species were produced simultaneously.   The mass pattern of H$^+$(H$_2$O)$_n$, in which $n = 20$ - 22 are highlighted in blue, shows the well-known magic number behavior at $n = 21$. [60 - 64] This magic number is attributed to the stable closed cage structure formation with one water molecule (or H$_3$O$^+$) inside the cage. [63 - 72]   On the other hand, for TMA-H$^+$-(H$_2$O)$_n$, of which the magic number region is highlighted in red, no clear magic number behavior is seen at $n = 21$ (and also at $n = 20$, as discussed

later). Figure 13 shows the observed IR spectra of TMA-H$^+$-(H$_2$O)$_n$ (n = 20 - 22) in the free OH stretching region . The spectra of H$^+$(H$_2$O)$_n$ are also shown for comparison. In the spectra of H$^+$(H$_2$O)$_n$, the intensity of the AD water band at 3715 cm^{-1} suddenly decreases and the AAD band at 3695 cm^{-1} becomes predominant at n = 21. Only closed polyhedral cages are possible structures if all the water molecules are three-coordinated. Therefore this spectral change at n = 21 is the spectroscopic signature of the closed cage formation at the magic number. [39-41] On the other hand, in the case of TMA-H$^+$-(H$_2$O)$_n$, such a spectral change is not observed at n = 21 (and also at n = 20). If the excess proton in TMA-H$^+$-(H$_2$O)$_n$, is transferred to the water moiety, the magic number behavior similar to H$^+$(H$_2$O)$_n$ is expected both in its mass and IR spectra. [20] In several mixed protonated clusters, such as (MeOH)$_m$-H$^+$(H$_2$O)$_n$, (NH$_3$)$_m$-H$^+$-(H$_2$O)$_n$, (monomethylamine)$_m$-H$^+$(H$_2$O)$_n$, and (tert-butanol)-H$^+$(H$_2$O)$_n$, the similar magic number behavior has actually been reported at m + n = 21. [29, 73-76] Therefore, the present results demonstrate that the excess proton would be located at the TMA moiety even at these large sizes.

Absence of the magic number behavior of TMA-H$^+$-(H$_2$O)$_n$ in mass spectrometry has been reported by Nguyen et al. [77] However, Chang et al. have recently reported the mass and IR spectra of TMA-H$^+$-(H$_2$O)$_n$ stored at 133 K, and they have

observed the magic number behavior both in the mass and IR spectra at $n = 20$. [29] The

clearness of the magic number behavior of TMA-H$^+$-(H$_2$O)$_{20}$ is weaker than those of

hydrated clusters of other protonated amines such as ammonia and monomethylamine

and they have suggested coexistence of several different types of isomers. This

observation by Chang *et al.* is quite contrastive to the present result. This difference

would be due to observation of different isomers induced by the different experimental

conditions; higher temperature (150 ~ 200 K) and shorter time scale (~ 100 μs) for IR

dissociation detection in our experiments and lower temperature (133 K) and longer

time scale (ms or longer) in the experiments by Chang *et al.*

      Here we comment on the specialty of the result reported by Chang *et al.* [29] To

form a stable cage structure for the magic number behavior in hydrated clusters with an

excess proton, total 21 molecules which can be compatible with water in H-bond

networks are requested. [63 – 76] 20 molecules form the cage and one molecule is located

inside the cage. To be compatible with water in the closed cage networks, the molecule

should be able to be three or four coordinated. Therefore, in X$_m$-H$^+$-(H$_2$O)$_n$ clusters,

mixing of water-compatible molecules, such as X = methanol, ammonia,

monomethylammonium, and tert-butanol leads the mixed clusters of total 21 molecules

($m + n = 21$) to the magic number behavior while the mixing of non-compatible

molecules results in the magic number behavior at 21 water molecules (X = phenyl

radical) or disappearance of the magic number behavior (X = tetramethylammonium

and dimethylamine). [20, 29, 73 - 76] TMA can only be one-coordinated in H-bond networks

and this molecule should be located at outside the H-bond networks (and its molecular

size is too large to be included in the cage formed by 20 water molecules). Therefore,

the origin of the magic number behavior of TMA-H$^+$-(H$_2$O)$_{20}$ should be different from

that of H$^+$(H$_2$O)$_{21}$.   There has been no report on the special stability of cages formed by

20 water molecules (with or without an excess proton) and the mechanism of the magic

number behavior of TMA-H$^+$-(H$_2$O)$_{20}$ should be totally new one.

Figure 14 shows the observed IR spectra of TMA-H$^+$-(H$_2$O)$_n$ (n =10, 15, 18, 20,

21) and H$^+$(H$_2$O)$_{21}$ in the full OH stretch region. The H-bonded OH stretch bands of

TMA-H$^+$-(H$_2$O)$_{21}$ are clearly different from those of H$^+$(H$_2$O)$_{21}$. This is also consistent

with the absence of the magic number behavior of TMA-H$^+$-(H$_2$O)$_{21}$ and indicates that

its H-bond network is different from that of H$^+$(H$_2$O)$_{21}$. In addition, the feature of

TMA-H$^+$-(H$_2$O)$_{21}$ is different also from that of the neutral water clusters around this size.

[47, 78 – 80] Though the water moiety would be neutral, its H-bond network is still

influenced by the excess proton even at this size. In the spectra of TMA-H$^+$-(H$_2$O)$_n$ (n =

10, 15, 18, 20, 21), the free OH stretching band at ~3700 cm^{-1} becomes sharper with

increasing cluster size. This is attributed to the reduction of the AD sites and the

predominance of the three-coordinated (AAD and ADD) sites in forming the closed

cage network structures. Moreover, the band at 3250 cm^{-1} become prominent at

TMA-H$^+$-(H$_2$O)$_{20-21}$. The H-bonded OH stretch region of the spectrum of

TMA-H$^+$-(H$_2$O)$_{20}$ under the magic number condition has been reported by Chang *et al.*

[29] Their spectrum is similar to the present one but the 3250 cm^{-1} band is more prominent.

This would be due to the difference of temperature of the observed clusters. Chang *et al.*

have reported that the band at 3250 cm^{-1} becomes prominent when a positively charged

site (metal cation or protonated site) is localized at the surface of H-bond networks

formed by 20 water molecules. [29] It would be, therefore, reasonable to assume that the

3250 cm^{-1} band is a marker of highly polarized H-bond networks to stabilize the excess

charge on the water surface at this size range. The mass and IR spectral features of

TMA-H$^+$-(H$_2$O)$_n$ in this study show that the excess proton of TMA-H$^+$-(H$_2$O)$_n$ is located

at the TMA moiety even in large sizes ($n = \sim20$) and the H-bond network is arranged to

have a large dipole moment to stabilize the neighboring excess proton.   Here we note

on an alternative interpretation.   If the excess proton is transferred to the water moiety

but TMA is directly bound to the produced hydronium ion as a proton acceptor, the

hydronium ion effectively behaves as a 2-coordinated site in the water network, and the

absence of the magic number behavior is reasonably explained.   The formation of the

highly polarized water network is concluded also in this interpretation.

Finally we comment on some important implications of the present results.

This H-bond network morphology of TMA-H$^+$-(H$_2$O)$_n$, which is arranged to have large

dipole moment in the water moiety, seems to be similar to that of the dipole-bound

water cluster anions (H$_2$O)$_n^-$. [16, 81] It is interesting that the IR spectra of

TMA-H$^+$-(H$_2$O)$_{20}$ and (H$_2$O)$_{20}^-$, which has been reported by Hammer *et al.*, [81] are

similar to each other in the H-bonded OH region and both of them show the remarkable

band at 3250 cm^{-1}. Though the 3250 cm^{-1} band in (H$_2$O)$_{20}^-$ has been assigned to the OH

stretches of the special water site which directly contacts with the excess electron, the

present results suggest alternative possibility that a highly polarized water network

shows a similar band.

Another implication is on the "titration" of the magic number cluster

H$^+$(H$_2$O)$_{21}$ with TMA, which has been reported by Wei *et al.* [64] They have reported mass

spectrometry of (TMA)$_n$-H$^+$-(H$_2$O)$_{21}$ to count the number of the dangling OH bond on

the surface of H$^+$(H$_2$O)$_{21}$, that is useful information to determine the excess proton

location. As a result, they have observed the drastic reduction of the production yield of

(TMA)$_n$-H$^+$-(H$_2$O)$_{21}$ at *n* = 11 and they have concluded that the magic number cluster

$H^+(H_2O)_{20}$ has 10 dangling OH bonds and therefore the H_3O^+ ion core is located at the center of the cage. However, they have discussed under the assumption that the excess proton is localized on the water moiety and the mixing of TMA does not change the H-bond network of the magic number cluster. In their experiment, the mixed cluster was formed by the ionization of the co-expansion of TMA and water (similar to the present study) and not by the pick-up techniques. [64] Therefore, the present study demonstrates the possibility that the water H-bond network probed by the previous titration experiment is different from that in the $H^+(H_2O)_{21}$ magic number cluster because of the localization of the excess proton at the TMA moiety.   The very recent mass spectrometric study on (tert-butanol)$_m$-H$^+$-(H$_2$O)$_n$ ($m + n = 21$) mixed clusters has indicated that there is only 9 dangling OH bonds in the magic number cluster and suggested the H$^+$TMA ion core formation in the titration experiment.[76]   The present study well-explains this inconsistency between the previous experiments on the dangling OH bond number determination.

IV. Summary

In this work, we studied size-dependent development of the H-bond network structures of TMA-H$^+$-(H$_2$O)$_n$ in the size range of $n = 1$ - 22. The detailed structures of the clusters

and the temperature dependence of the isomer population were discussed up to $n = 6$.

For TMA-H$^+$-(H$_2$O)$_n$ (n = 1-22), no evidence of the proton transfer to the water moiety was found and the excess proton is considered to be always localized at the TMA moiety. The observed IR spectra of TMA-H$^+$-(H$_2$O)$_n$ are different from those of H$^+$(H$_2$O)$_n$ and (H$_2$O)$_n$. Thus the H-bond network structures of TMA-H$^+$-(H$_2$O)$_n$ are neutral but are under the strong influence of the excess proton. Moreover, the H-bond networks are arranged to have large dipole moment at the water moiety to stabilize the excess proton localized at the TMA moiety. This morphology of the water networks is different both from H$^+$(H$_2$O)$_n$ and (H$_2$O)$_n$, but is similar to dipole-bound (H$_2$O)$_n^-$. The H-bond network structures of TMA-H$^+$-(H$_2$O)$_n$ (n = 1-3) have chain or tree type networks. The single and double ring type networks begin to appear at n = 4 and 6, respectively. The single ring type networks become dominant in n = 5, while dominance of the double ring type with minor contribution of the single ring type is demonstrated in n = 6. The excess proton would not be transferred to the water moiety even in larger size ($n \sim 20$), and the excess proton still causes prominent alignment of the H-bond networks. Some implications of the present results were commented on the relation to IR spectroscopy of water anion clusters and the titration experiments of the magic number cluster of protonated water.

Electronic Supplementary Information (ESI) available: Number of the stable isomers of TMA-H$^+$-(H$_2$O)$_n$ (n = 3 − 6), relative energies of the isomers, comparison between the B3LYP and ωB97xD calculations results, and complete calculation data sets on dependence of the magnitudes of dipole moment on their morphology.

References

1. D. R. Lide (Ed.), CRC Handbook of Chemistry and Physics 90th Edition, CRC Press, Boca Raton, 2009.

2. D. Eisenberg, W. J. Kauzmann, The Structure and Properties of water, Oxford at the

Clarendon Press, London, 1969.

3. J. N. Israelachvili, Intermolecular and Surface Forces, Third edition, Elsevier Inc., Burlington, 2011.

4. P. Hobza, K. Müller-Dethlefs, Non-Covalent Interactions: Theory and Experiment, Royal Society of Chemistry, Nottingham, 2010.

5. E. D. Glendening, D. Feller, *J. Phys. Chem.* 1995, **99**, 3060-3067.

6. H. C. Chang, Y. S. Wang, Y. T. Lee, H. C. Chang, *Int. J. Mass Spectrometry* 1998, **180**, 91-102.

7. R. S. Walters, E. D. Pillai, M. A. Duncan, *J. Am. Chem. Soc.* 2005, **127**, 16599-16610.

8. A. Fujihara, C. Miyata, A. Maekawa, K. Fuke, K. Daigoku, N. Murata, K. Hashimoto, *J. Phys. Chem. A* 2007, **111**, 7364-7373.

9. T. Iino, K. Ohashi, K. Inoue, K. Judai, N. Nishi, H. Sekiya, *J. Chem. Phys*. 2007, **126**, 194302.

10. D. J. Miller, J. M. Lisy, *J. Am. Chem. Soc.* 2008, **130**, 15381-15392.

11. M. F. Bush, R. J. Saykally, E. R. Williams, *J. Am. Chem. Soc.* 2008, **130**, 15482-15489.

12. D. J. Goebbert, E. Garand, T. Wende, R. Bergmann, G. Meijer, K. R. Asmis, D. M.

Neumark, *J. Phys. Chem. A* 2009, **113** , 7584-7592.

13. E. Garand, T. Wende, D. J. Goebbert, R. Bergmann, G. Meijer, D. M. Neumark, K. R. Asmis, *J. Am. Chem. Soc.* 2010, **132**, 849-856.

14. M. Alauddin, J. K. Song, S. M. Park, *Int. J. Mass Spectrometry* 2012, **314**, 49-56.

15. M. Schmies, M. Miyazaki, M. Fujii, O. Dopfer, *J. Chem. Phys*. 2014, **141**, 214301.

16. N. I. Hammer, J. W. Shin, J. M. Headrick, E. G. Diken, J. R. Roscioli, G. H. Weddle, M. A. Johnson, *Science* 2004, **306** , 675-679.

17. T. Sawamura, A. Fujii, S. Sato, T. Ebata, N. Mikami, *J. Phys. Chem*. 1996, **100**, 8131-8138.

18. M. Miyazaki, A. Fujii, T. Ebata, N. Mikami, *Phys. Chem. Chem. Phys.* 2003, **5**, 1137-1148.

19. M. Miyazaki, A. Fujii, T. Ebata, N. Mikami, *Chem. Phys. Lett.* 2004, **399**, 412-416.

20. M. Miyazaki, A. Fujii, T. Ebata, N. Mikami, *J. Phys. Chem. A* 2004, **108**, 10656-10660.

21. E. P. Hunter, S. G. Lias, *J. Phy. Chem. Ref. Data* 1998, **27**, 413-457.

22. S. Wei, W. B. Tzeng, A. W. Castleman Jr., *Chem. Phys. Lett*. 1991, **178**, 411- 418.

23. H. -C. Chang, J. -C. Jang, I. Hahndorf, S. H. Lin, Y. T. Lee, H. -C. Chang, *J. Am. Chem. Soc.* 1999, **121**,4443-4450.

24. G. H. Gardenier, J.R. Roscioli, M.A. Johnson, *J. Phys. Chem. A* 2006, **112**, 12022-12026.

25. T. C. Cheng, B. Bandyopadhyay, J. D. Mosley, M. A. Duncan, *J. Am. Chem. Soc.* 2012, **134**, 13046-13055.

26. I. Alata, M. Broquier, C. Dedonder-Lardeux, C. Jouvet, M. Kim, W. Y. Sohn, S. -S. Kim, H. Kahn, M. Schutz, A. Patzer, O. Dopfer, *J. Chem. Phys.* 2011, **134**, 074307.

27. D. Bing, T. Hamashima, C. W. Tsai, A. Fujii, J. –L. Kuo, *Chem. Phys.* 2013, **421**, 1-9.

28. R. Shishido, J. –L. Kuo, A. Fujii, *J. Phys. Chem. A* 2012, **116**, 6740-6749.

29. T. M. Chang, R. J. Cooper, E. R. Williams, *J. Am. Chem. Soc.* 2013, **135**, 14821-14830.

30. Q. C. Nguyen, Y. –S. Ong, H. Soh, and J. –L. Kuo, *J. Phys. Chem. A* 2008, **112**, 6257-6261.

31. Q. C. Nguyen, Y. –S. Ong, J. –L. Kuo, *J. Chem. Theory and Comp.* 2009, **5**, 2629-2639.

32. J. C. Jiang, Y. S. Wang, H. C. Chang, S. H. Lin, Y. T. Lee, G. Niedner-Schatteburg, *J. Am. Chem. Soc.* 2000, **122**, 1398−1410.

33. J. D. Chai, M. Head-Gordon, *Phys. Chem. Chem. Phys.* 2008, **10**, 6615-6620.

34. M. J. Frisch, G. W. Trucks, H. B. Schlegel, G. E. Scuseria, M. A. Robb, J. R. Cheeseman, G. Scalmani, V. Barone, B. Mennucci, G. A. Petersson, H. Nakatsuji, M. Caricato, X. Li, H. P. Hratchian, A. F. Izmaylov, J. Bloino, G. Zheng, J. L. Sonnenberg, M. Hada, M. Ehara, K. Toyota, R. Fukuda, J. Hasegawa, M. Ishida, T. Nakajima, Y. Honda, O. Kitao, H. Nakai, T. Vreven, J. Montgomery, J. E. Peralta, F. Ogliaro, M. Bearpark, J. J. Heyd, E. Brothers, K. N. Kudin, V. N. Staroverov, R. Kobayashi, J. Normand, K. Raghavachari, A. Rendell, J. C. Burant, S. S. Iyengar, J. Tomasi, M. Cossi, N. Rega, N. J. Millam, M. Klene, J. E. Knox, J. B. Cross, V. Bakken, C. Adamo, J. Jaramillo, R. Gomperts, R. E. Stratmann, O. Yazyev, A. J. Austin, R. Cammi, C. Pomelli, J. W. Ochterski, R. L. Martin, K. Morokuma, V. G. Zakrzewski, G. A. Voth, P. Salvador, J. J. Dannenberg, S. Dapprich, A. D. Daniels, O. Farkas, J. B. Foresman, J. V. Ortiz, J. Cioslowski, D. J. Fox, Gaussian 09, Revision B.01, Gaussian, Inc., Wallingford CT, 2009.

35. P. Flukiger, H. P. Luthi, S. Portmann and J. Weber, MOLEKEL 4.3, Swiss Center for Scientific Computing, Manno (Switzerland), 2000–2002.

36. T. Hamashima, Y. –C. Li, M. C. H. Wu, K. Mizuse, T. Kobayashi, A. Fujii, J. –L. Kuo, *J. Phys. Chem. A* 2013, **117**, 101-107.

37. Y. L. Cheng, H. Y. Chen, K. Takahashi, *J. Phys. Chem. A* 2011, **115**, 5641−5653.

38. M. Morita, K. Takahashi, *Phys. Chem. Chem. Phys*. 2012, **14**, 2797−2808.

39. M. Miyazaki, A. Fujii, T. Ebata, N. Mikami, *Science* 2004, **304**, 1134-1137.

40. J. W. Shin, N. I. Hammer, E. G. Diken, M. A. Johnson, R. S.Walters, T. D. Jaeger, M.
A. Duncan, R. A. Christie, K. D. Jordan, *Science* 2004, **304**, 1137-1140.

41. H. -C. Chang, C. -C. Wu, J. –K. Kuo, *Int. Rev. Phys. Chem.* 2005, **24**, 553-578.

42. C. –K. Lin, C. –C. Wu, Y. –S. Wang, Y. T. Lee, H. –C. Chang, J. –L. Kuo, M. L.
Klein, *Phys. Chem. Chem. Phys*. 2005, **7**, 938 – 944.

43. K. Mizuse, J. –L. Kuo, A. Fujii, *Chem. Sci*. 2011, **2**, 868-876.

44. Y. S. Wang, J. C. Jiang, C. L. Cheng, S. H. Lin, Y. T. Lee, H. -C. Chang, *J. Chem.
Phys*. 1997, **107**, 9695-9698.

45. J. C. Jiang, J. C. Chang, B. C. Wang, S. H. Lin, Y. T. Lee, H. -C. Chang, *Chem. Phys.
Lett*. 1998, **289**, 373-382.

46. U. Buck, F. Huisken, *Chem.Rev.* 2000*, **100**, 3863-3890.

47. V. Buch, S. Bauerecker, J. P. Devlin, U. Buck, J. Kazimirski, *Int. Rev. Phys. Chem*.
2004, **23**, 375-433.

48. T. Watanabe, T. Ebata, S. Tanabe, N. Mikami, *J. Chem. Phys*. 1996, **105**, 408-419.

49. R. N. Pribble, T. S. Zwier, *Science*, 1994, **265**, 75-79.

50. Ch. Janzen, D. Spangenberg, W. Roth, K. Kleinermanns, *J. Chem. Phys*. 1999, **110**,

9898-9907.

51. K. Mizuse, T. Hamashima, A. Fujii, *J. Phys. Chem. A* 2009, **113**, 12134-12141.

52. G. Hincapié, N. Acelas, M. Castaño, J. David, A. Restrepo, *J. Phys. Chem. A* 2010, **114**, 7809-7814.

53. C. Pérez, M. T. Muckle, D. P. Zaleski, N. A. Seifert, B. Temelso, G. C. Shields, Z. Kisiel, B. H. Pate, *Science*,2012, **336**, 897-901.

54. J. M. Headrick, E. G. Diken,1 R. S. Walters, N. I. Hammer, R. A. Christie, J. Cui, E. M. Myshakin, M. A. Duncan, M. A. Johnson, K. D. Jordan, *Science*, 2005, **308**, 1765-1769.

55. G. E. Douberly, A. M. Ricks, M. A. Duncan, *J. Phys. Chem. A* 2009, **113**, 8449−8453.

56. G. E. Douberly, R. S. Walters, J. Cui, K. D. Jordan, M. A. Duncan, *J. Phys. Chem. A* 2010, **114**, 4570−4579.

57. K. Mizuse, A. Fujii, *Phys. Chem. Chem. Phys*. 2011, **13**, 7129-7135.

58. K. Mizuse, A. Fujii, *J. Phys. Chem. A* 2012, **116**, 4868-4877.

59. N. Heine, M. R. Fagiani, M. Rossi, T. Wende, G. Berden, V. Blum, K. R. Asmis, *J. Am. Chem. Soc*. 2013, **135**, 8266.

60. S. −S. Lin, *Rev. Sci. Instrum*. 1973, **44**, 516-517.

61. J. Q. Searcy, J. B. Fenn, *J. Chem. Phys.* 1974, **61**, 5282-5288.

62. J. L. Kassner, D. E. Hagen, *J. Chem. Phys*. 1976, **64**, 1860-1861.

63. U. Nagashima, H. Shinohara, N. Nishi, H. Tanaka, *J. Chem. Phys*.1986, **84**, 209-214.

64. S. Wei, Z. Shi, A. W. Castleman, Jr., *J. Chem. Phys.* 1991, **94** , 3268-3270.

65. K. Laasonen, M. L. Klein, *J. Phys. Chem*. 1994, **98**, 10079−10083.

66. S. McDonald, L. Ojamäe, S. J. Singer, *J. Phys. Chem. A* 1998, **102**, 2824−2832.

67. M. P. Hodges, D. J. Wales, *Chem. Phys. Lett*. 2000, **324**, 279−288.

68. A. Khan. *Chem. Phys. Lett*. 2000, **319**, 440−450.

69. N. J. Singh, M. Park, S. K. Min, S. B. Suh, K. S. Kim, *Angew. Chem. Int. Ed*. 2006, **45**, 3795-3800.

70. T. Kus, V. F. Lotrich, A. Perera, R. J. Bartlett, *J. Chem. Phys*. 2009, **131**, 104313.

71. S. S. Xantheas, *Can. J. Chem. Eng*. 2012, **90**, 843−851.

72. T.-H. Choi and K. D. Jordan, *J. Phys. Chem. B*, 2010, **114**, 6932-6936.

73. Z. Shi, S. Wei, J. V. Ford, A. W. Castleman Jr., *Chem. Phys. Lett*. 1992, **200**, 142 -146.

74. K. Suhara, A. Fujii, K. Mizuse, N. Mikami, J. –L. Kuo, *J. Chem. Phys.* 2007, **126**, 194306.

75. E. G. Diken, N. I. Hammer, M. A. Johnson, R. A. Christie, K. D. Jordan, *J. Chem. Phys.* 2005, **123**, 164309.

76. M. J. Ryding, R. Izsák, P. Merlot, S. Reine, T. Helgaker, E. Uggerud, *Phys. Chem. Chem. Phys.* 2015, **17**, 5466-5473.

77. V. Q. Nguyen, X. G. Chen, A. L. Yergey, *J. Am. Soc. Mass Spectrometry* 1997, **8**, 1175-1179.

78. T. Hamashima, K. Mizuse, A. Fujii, *J. Phys. Chem. A* 2011, **115**, 620-625.

79. C. C. Pradzynski, M. Forck, T. Zeuch, P. Slavíček, U. Buck, *Science*, 2012, **337**, 1529-1532.

80. C. C. Pradzynski, C. W. Dierking, F. Zurheide, R. M. Forck, U. Buck, T. Zeuch, S. S. Xantheas. *Phys. Chem. Chem. Phys.* 2014, **16**, 26691-26696.

81. N. I. Hammer, J. R. Roscioli, J. C. Bopp, J. M. Headrick, M. A. Johnson, *J. Chem. Phys.* 2005, **123** , 244311.
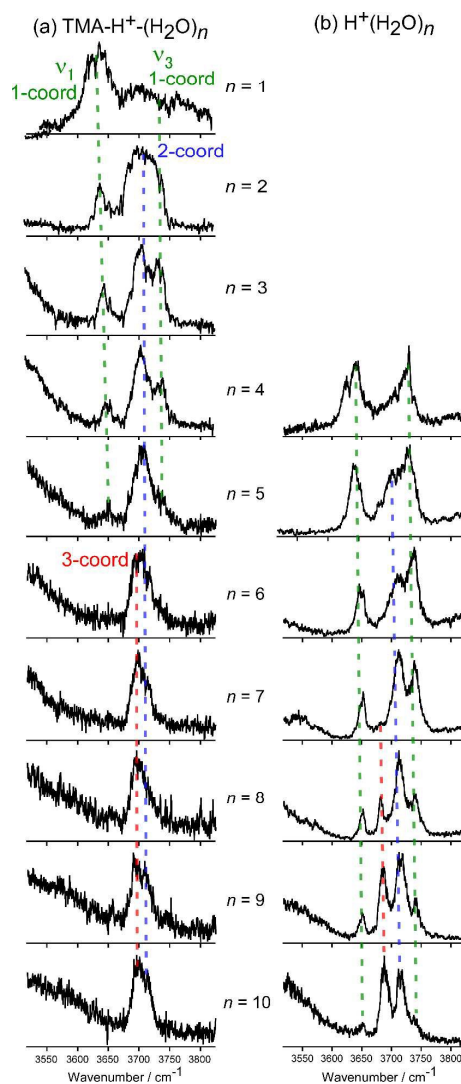
Figure 1   Infrared (IR) spectra of (a) TMA-H$^+$-(H$_2$O)$_n$ and (b) H$^+$(H$_2$O)$_n$ in the free

OH stretch region. Bands at 3640 and 3740 cm^{-1} (labeled by the green dotted lines) are

ν_1 and ν_3 vibrations of a single acceptor (A) water site in a H-bond chain. Bands at

3715 cm^{-1} (labeled by the blue dotted line) and 3695 cm^{-1} (red dotted line) are attributed

to dangling OH stretches of two-coordinated (AD) and three-coordinated (AAD) water

sites, respectively.

40
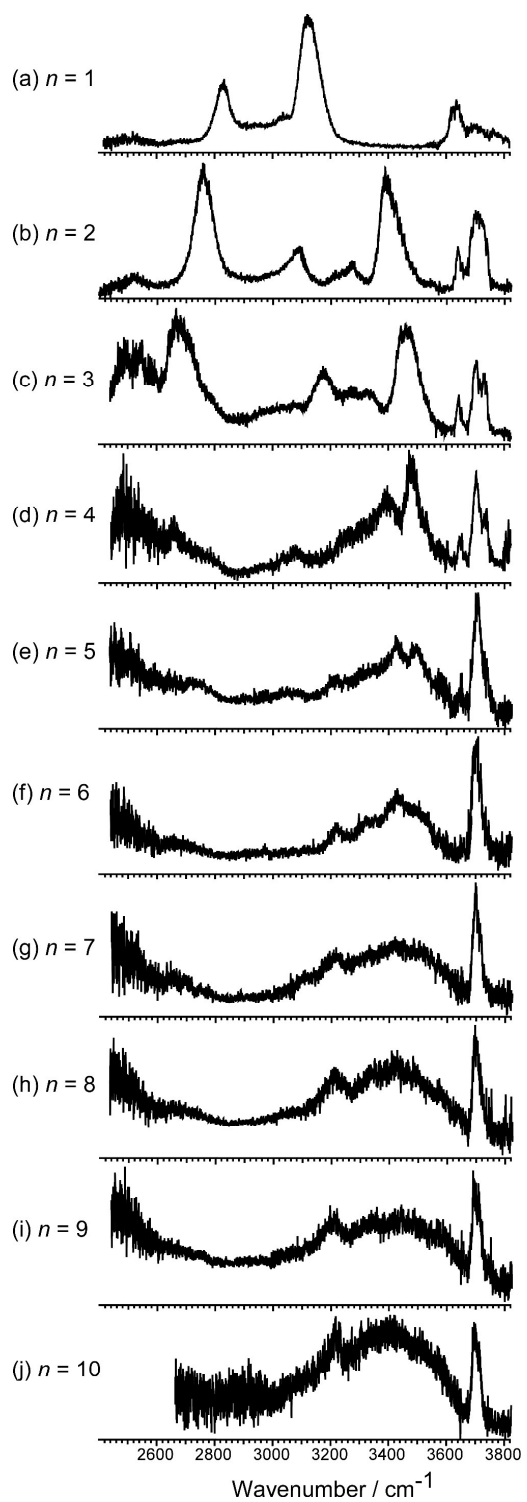
Figure 2   IR spectra of TMA-H$^+$-(H$_2$O)$_n$ (n = 1-10). The spectra were obtained by

monitoring the TMA-H$^+$-(H$_2$O)$_{n-1}$ fragment while scanning the IR wavelength.

41
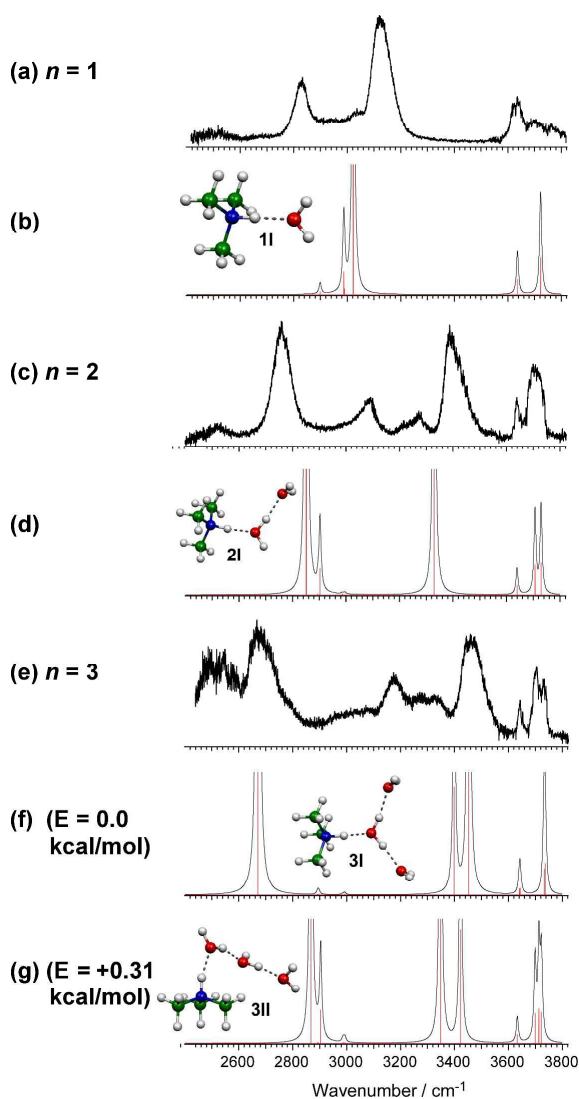
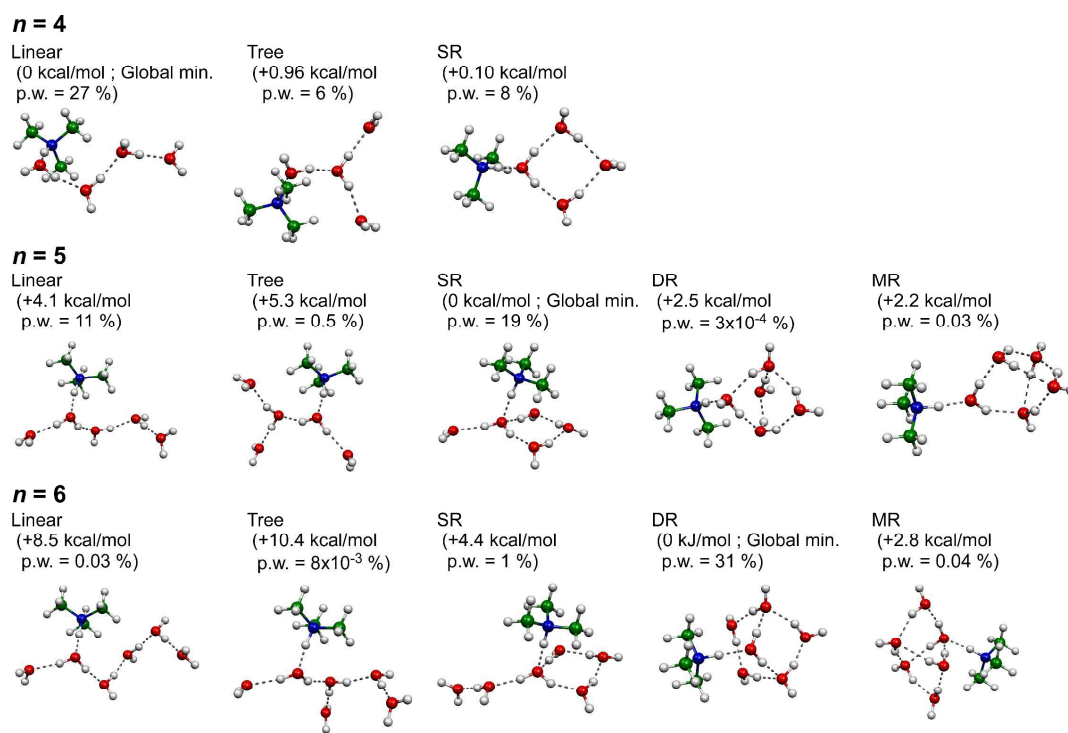**Figure 3** Comparison among the observed IR spectra of TMA-H$^+$-(H$_2$O)$_n$ ($n = 1$

– 3) and their simulated IR spectra based on the optimized stable structures. All the

calculations were performed at the ωB97xD/6-311+G(2d,p) level. In the simulation,

the scaling factor of 0.9394 is applied to the calculated harmonic frequencies. For $n =$

3, the relative energies between the isomers are also shown. The Cartesian coordinates
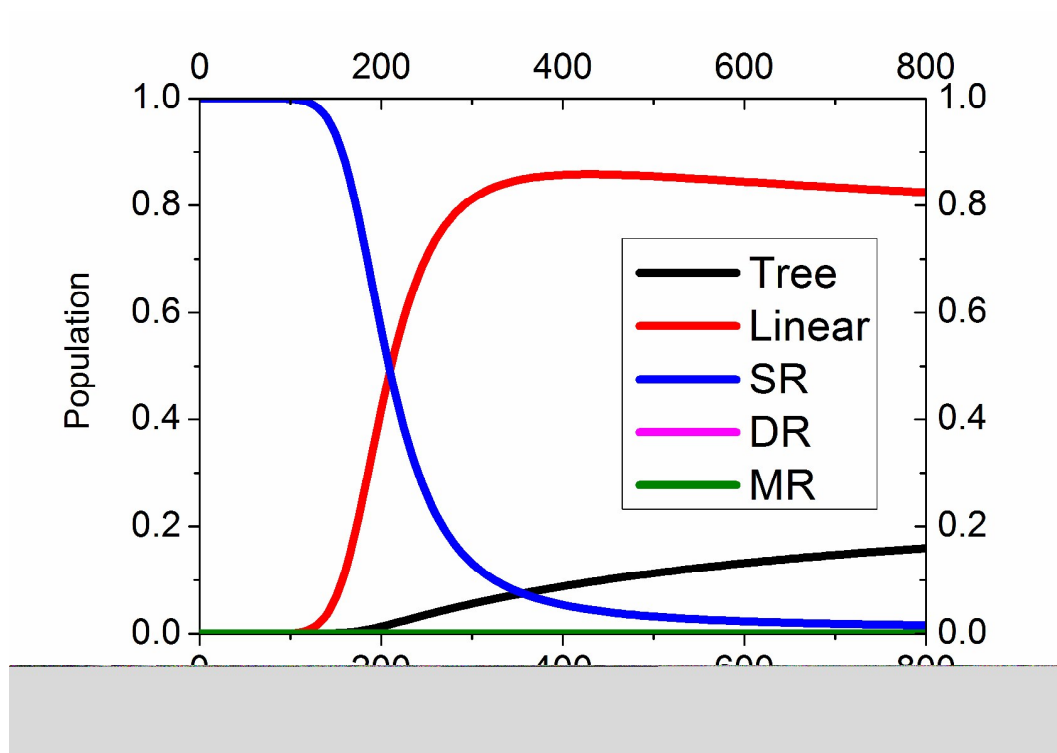
of the stable structures are provided in ESI.
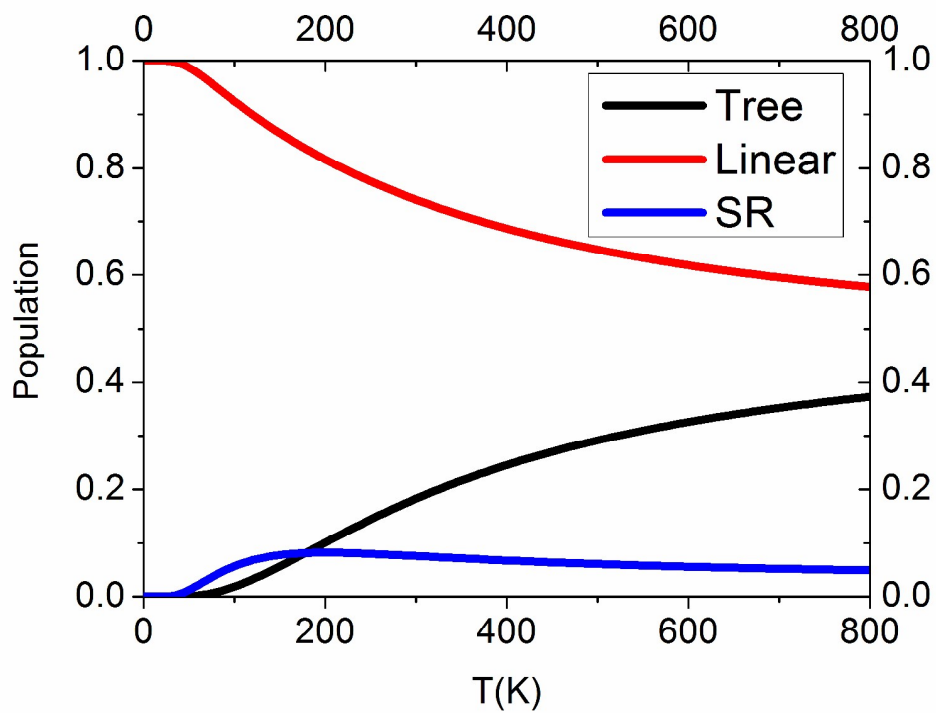
Figure 4   Temperature dependecne of the isomer populations of $n = 4$.   Each curve shows the total sum of the relative population weights of isomers of the same morphology group. All the calculations were performed at the ωB97xD/6-311+G(2d,p) level with the harmonic approximation.
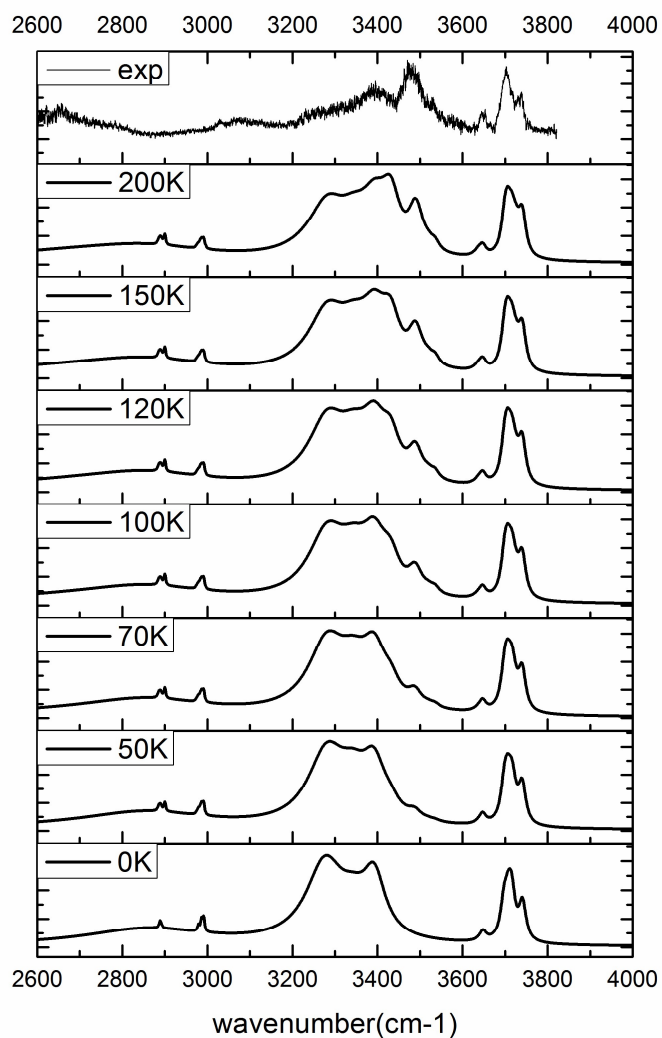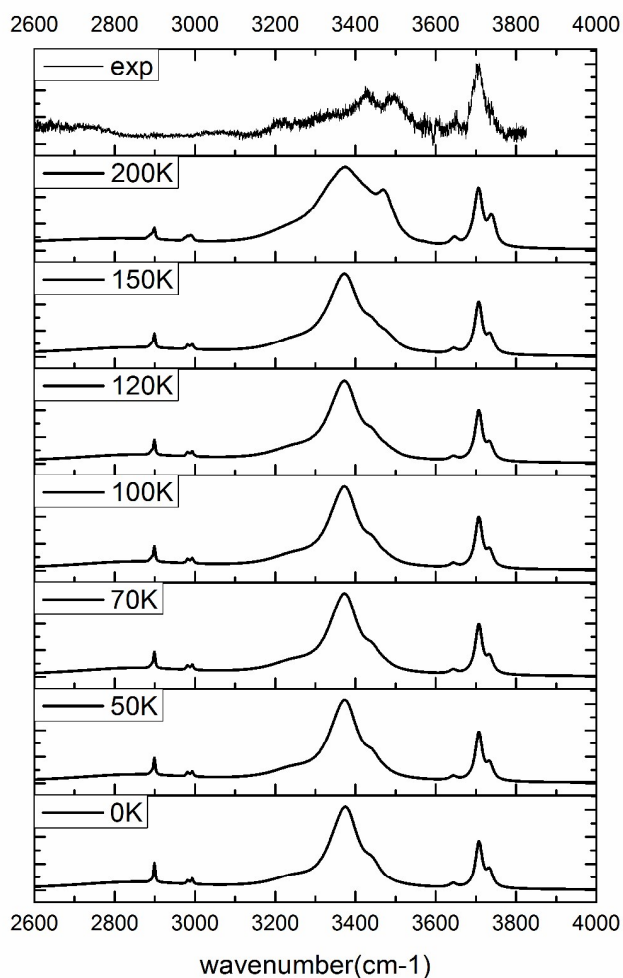
Figure 5   Temperature dependence of the IR spectral simulations of $n = 4$ by the

Q-HSA.   The isomer populations are based on those represented in Figure 4.   In the

simulation, the scaling factor of 0.9394 is applied to the calculated harmonic

frequencies.

n = 4

Linear
(0 kcal/mol ; Global min.
p.w. = 27 %)

Tree
(+0.96 kcal/mol
p.w. = 6 %)

SR
(+0.10 kcal/mol
p.w. = 8 %)

n = 5

Linear
(+4.1 kcal/mol
p.w. = 11 %)

Tree
(+5.3 kcal/mol
p.w. = 0.5 %)

SR
(0 kcal/mol ; Global min.
p.w. = 19 %)

DR
(+2.5 kcal/mol
p.w. = 3×10^{-4} %)

MR
(+2.2 kcal/mol
p.w. = 0.03 %)

n = 6

Linear
(+8.5 kcal/mol
p.w. = 0.03 %)

Tree
(+10.4 kcal/mol
p.w. = 8×10^{-3} %)

SR
(+4.4 kcal/mol
p.w. = 1 %)

DR
(0 kJ/mol ; Global min.
p.w. = 31 %)

MR
(+2.8 kcal/mol
p.w. = 0.04 %)

Figure 6   Sstructures of the global minimum isomers of TMA-H$^+$-(H$_2$O)$_n$ (*n* = 4 –

6) with those of the most populated isomer in each morphology type at 200 K. Numbers

in parentheses are energy relative to the global minimum in each size and population

weight at 200 K.   The Cartesian coordinates of the stable structures are provided in

ESI.

Figure 7 Temperature dependecne of the isomer populations of $n = 5$. Each

curve shows the total sum of the relative population weights of isomers of the same

morphology group. All the calculations were performed at the ωB97xD/6-311+G(2d,p)

level with the harmonic approximation.

Figure 8　　　Temperature dependence of the IR spectral simulations of *n* = 5 by the

Q-HSA.　　The isomer populations are based on those represented in Figure 7.　　In the

simulation, the scaling factor of 0.9394 is applied to the calculated harmonic

frequencies.
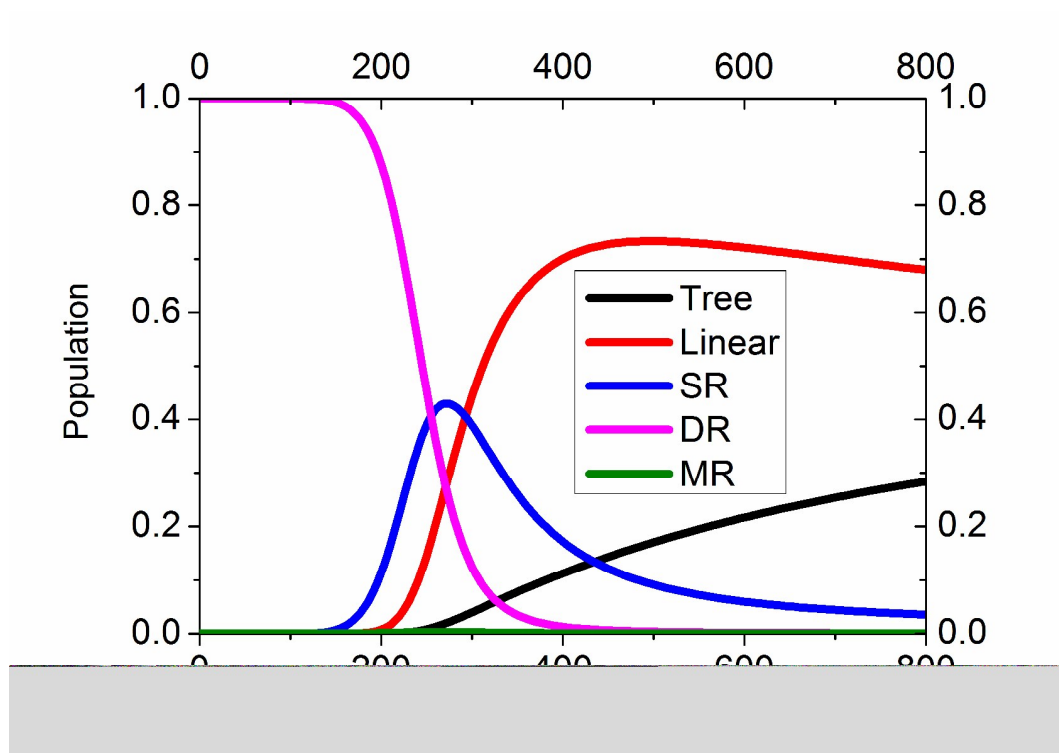
Figure 9   Temperature dependecne of the isomer populations of *n* = 6.   Each

curve shows the total sum of the relative population weights of isomers of the same

morphology group. All the calculations were performed at the ωB97xD/6-311+G(2d,p)

level with the harmonic approximation.
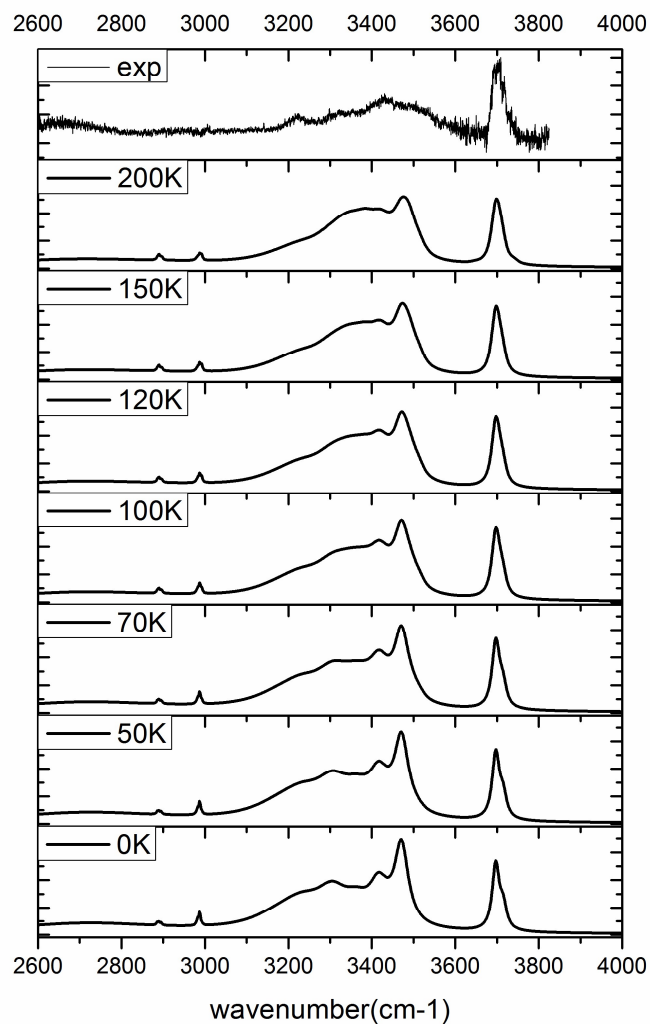
Figure 10 Temperature dependence of the IR spectral simulations of *n* = 6 by the

Q-HSA. The isomer populations are based on those represented in Figure 9. In the

simulation, the scaling factor of 0.9394 is applied to the calculated harmonic

frequencies.
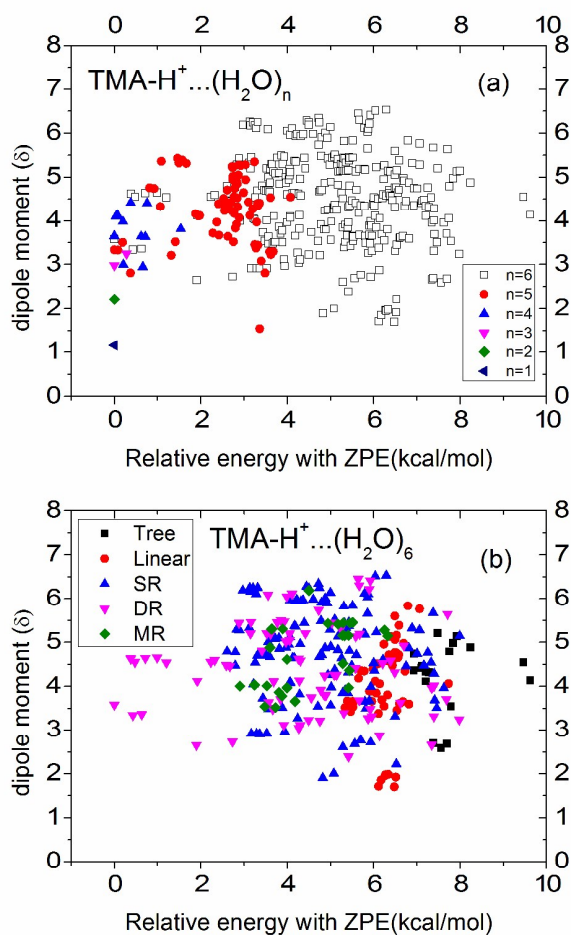
Figure 11 (a) Estimated dipole moment of the water moiety versus relative energy of the stable structures for TMA-H$^+$-(H$_2$O)$_n$ (n = 1 – 6). Averaged dipole moment has increased from 1.2δ (n = 1), 2.3δ (n = 2) to ~3.0 δ (n = 3). At sizees n = 4 to n = 6, most isomers have ~4.0 δ regardless their stability. Definition of δ can be found in the main text. (b) Dependence of the magnitudes of dipole on their morphology for n = 6. A complete set of results for n = 4 to n = 6 can be found in ESI.
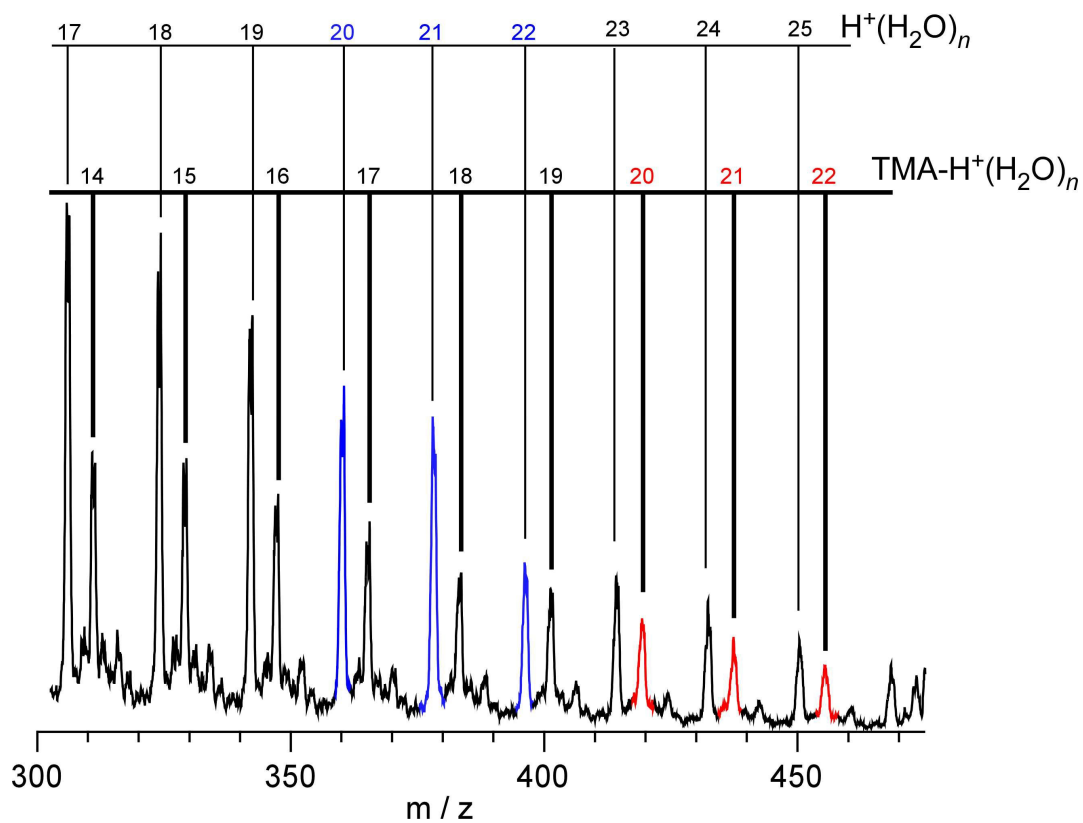
Figure 12   Mass spectrum of $H^+(H_2O)_n$ and $TMA\text{-}H^+\text{-}(H_2O)_n$ produced by co-expansion of the TMA/H$_2$O/Ar mixture and discharge. The magic number appears at $n = 21$ of $H^+(H_2O)_n$.

(a) TMA-H$^+$-(H$_2$O)$_n$ (b) H$^+$(H$_2$O)$_n$

n = 20

n = 21

n = 22

Wavenumber / cm^{-1} Wavenumber / cm^{-1}
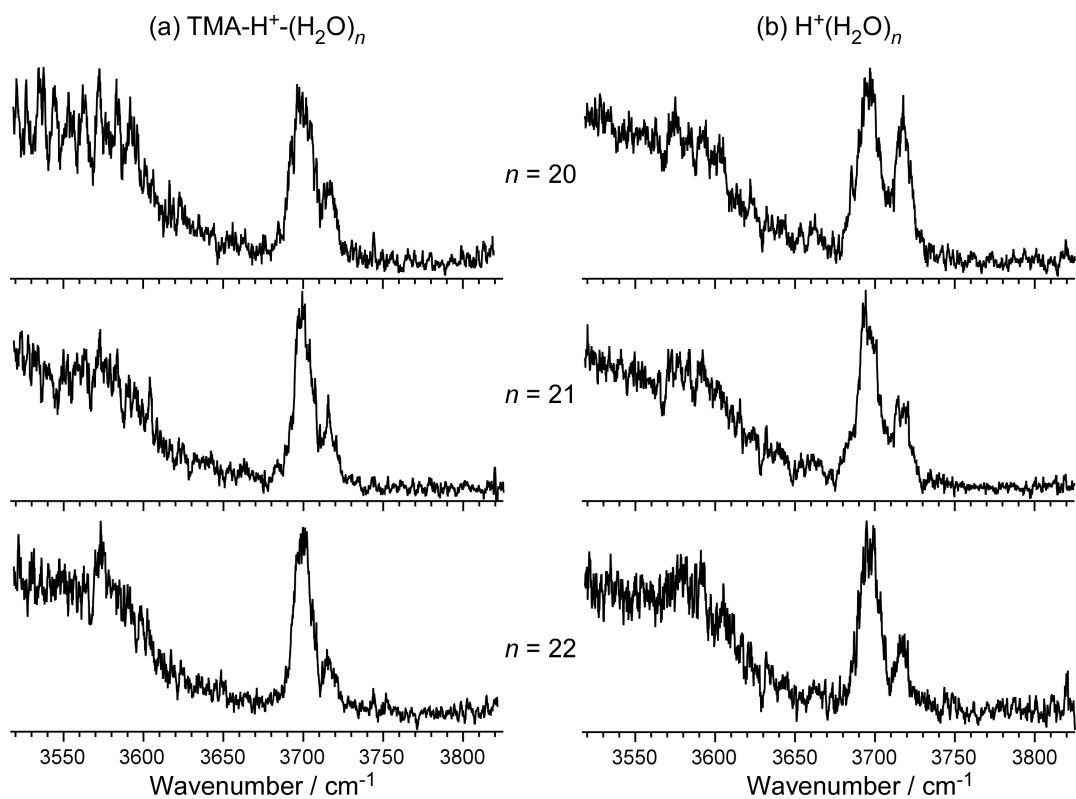
Figure 13   Observed IR spectra of (a) TMA-H$^+$-(H$_2$O)$_n$ and (b) H$^+$(H$_2$O)$_n$ (*n* = 20-22) in the free OH stretch region.
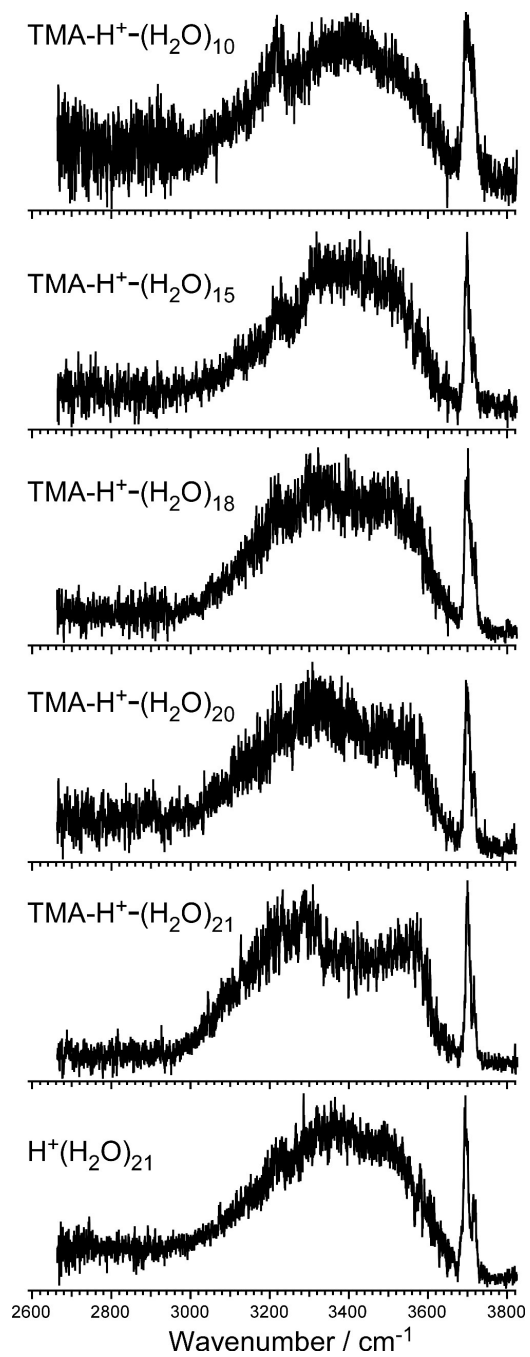
Figure 14   Observed IR spectra of TMA-H$^+$-(H$_2$O)$_n$ (n = 10,15,18,20, and 21) and

H$^+$(H$_2$O)$_n$ (n = 21).